Technology in Cancer Research and Treatment
ISSN 1533-0346
Volume 11, Number 2, April 2012

Towards Electroporation Based Treatment Planning Considering Electric Field Induced Muscle Contractions

www.tcrt.org

Alex Golberg, Ph.D.*
Boris Rubinsky, Ph.D.

Department of Mechanical Engineering, Etcheverry Hall, 6124, University of California at Berkeley, Berkeley, CA 94720, USA

The electric field threshold for muscle contraction is two orders of magnitudes lower than that for electroporation. Current electroporation treatment planning and electrode design studies focus on optimizing the delivery of electroporation electric fields to the targeted tissue. The goal of one part of this study was to investigate the relation between the volumes of tissue that experience electroporation electric fields in a targeted tissue volume and the volumes of tissue that experience muscle contraction inducing electric fields around the electroporated tissue volume, (V_{MC}), during standard electroporation procedures and for various electroporation electrodes designs. The numerical analysis shows that conventional electroporation protocols and electrode design can generate muscle contraction inducing electric fields in surprisingly large volumes of non-target tissue, around the electroporation treated tissue. In studying various electrode configurations, we found that electrode placement in a structure we refer to as a "Current Cage" can substantially reduce the volume of non-target tissue exposed to electric fields above the muscle contraction threshold. In an experimental study on a tissue phantom we compare a commercial two parallel needle electroporation system with the Current Cage design. While tissue electroporated volumes were similar, V_{MC} of tissue treated using the Current Cage design electrodes was an order of magnitude smaller than that using a commercially available system. An important aspect of the entire study is that it suggests the benefit of including the calculations of V_{MC} for planning of electroporation based treatments such as DNA vaccination, electrochemotherapy and irreversible electroporation.

Key words: Electroporation; DNA vaccination; Electrochemotherapy; Electrode configuration; Muscle contraction; Current Cage.

Introduction

When certain electric fields are applied across a cell, they have the ability to permeabilize the cell membrane, presumably through the formation of nanoscale defects- pores- in the membrane. The process of cell membrane permeabilization by pulsed electric fields (PEF) is coined "electroporation" (1). Electroporation is reversible when cells survive the electropermeabilization and irreversible when they do not. The relations between pulse electric field parameters such as field amplitude, pulse duration and number of pulses and electroporation phenomena were recently reported by (2, 3) and (4).

Reversible electroporation has become an important tool in biotechnology and medicine (5). It facilitates the introduction of otherwise non-permeable external substances into cells while keeping cells alive. Applications of reversible electroporation include gene delivery to cells (1) and tissues (6), and the introduction

*Corresponding author:
Alex Golberg, Ph.D.
E-mail: alex.golberg@berkeley.edu

of drugs into cells (7). Reversible electroporation is the basis for a successful cancer treatment therapy known as "electrochemotherapy" (8). Electrochemotherapy is a regional tumor treatment procedure that uses pulse electric field to increase the uptake of non-permeant, cytotoxic drugs (9, 10). The increase of up to three orders of magnitude was observed for bleomycin after the applications of pulse electric fields (11, 12). In addition, reversible electroporation is used in DNA vaccination to increase intracellular delivery of vaccine plasmid (13, 14). Animal studies show that reversible electroporation increases by two orders of magnitude the expression levels of the DNA vaccines (15). Moreover, NIH reports on more than 17 clinical studies on the use of electroporation for mediated DNA vaccination (16). While reversible electroporation is very successful in the designated applications, reports show that muscle contraction and pain is an undesirable side effect of reversible electroporation (17-19).

Recently, non-thermal irreversible electroporation (NTIRE) has emerged as a new clinical technique for tissue ablation (20, 21). The target cells are destroyed through the application of certain high strength, short duration pulsed electric fields that NTIRE (22, 23). The NTIRE pulses are chosen in such a way as to avoid Joule heating induced thermal damage (24, 25). The pulses are delivered through electrodes in contact with the targeted tissue (26). The important distinguished property of NTIRE tissue ablation is that other cells' structures, such as blood vessels scaffold and nerves, remain intact and neighboring cells are not affected (21, 27, 28). Successful treatments of prostate, liver, lung, kidney, breast and brain tumors were performed (29, 30). Despite its advantages, side effects and limitations of NTIRE were also reported (21, 31-33). The most severe of them are arrhythmias and involuntary muscle twitches, which may cause to electrode dislocation between the pulses (21, 31-33). The solution to arrhythmias through a synchronizer device is described in (32) and (33). Although strong paralytics such as *cisatracurium* or *rocuronium* (21, 32) and deep anesthesia are used in clinical NTIRE treatments, muscle contractions are still observed in the proximity to the electrodes; moreover, diaphragm contractions still take place (32).

Muscles and nerves are excitable tissues, therefore they respond to electric stimulation by contractions and pain. It was shown that a muscle twitch is the result of three mechanisms related to electric currents and fields. First, a twitch results from a multiple involuntary spinal reflex response (through peripheral nerves or primarily motor nerves) (34, 35). Second, contractions may result from direct motor-neuron electrical stimulation in the region of electrode contact (34). Third, it was found that contractions may also result from a direct electrical stimulation of denerved muscles (17). Strength-duration curves of muscle contraction show that pulse duration shortening from 10^3 μs to 10^{-3} μs increased the electric field strength threshold for muscle activation from 5 V/cm to $5{\cdot}10^4$ V/cm (36). Moreover, Joshi *et al.* (35) showed that specific pulse electric field parameters cause muscle contraction inhibition. Electrochemotherapy and DNA electro vaccination related pain and unpleasant sensations were investigated by (14, 17-19, 37).

Recently, several studies tried to address the issue of Electrochemotherapy and DNA electrovaccination induced muscle contraction and pain by using local anesthesia, modification of electroporation protocol (17, 37) and electrode design (38). It was found that local anesthesia by lidocaine was not successful to reduce the pain or prevent muscle contraction during electrochemotherapy (39-41). Furthermore, in our recent rat animal studies, intra muscular and spinal injection of lidocaine did not prevent strong muscle contractions during NTIRE (unpublished). An attempt at increasing the frequency of pulse delivery to 5 kHz led to a beneficial tetanus contraction of a rat's muscle during electrochemotherapy treatments instead of several independent contractions (17). Human response comparison between 5 kHz and 1 Hz protocols have shown that 5 kHz pulses were less unpleasant than 1 Hz pulses; however, the pain intensity was the same (37). Electroporation based DNA vaccination optimization experiments reveal that an increase in pulse delivery frequency and the shortening of the pulse duration, in combination with topical anesthesia, emla cream, decrease the strength of muscle twitches and increase the tolerance to the electroporation based vaccination procedure (18).

Zupanic *et al.* (37) suggested that the unpleasant sensation can be reduced by changing of the electrode geometry. Indeed, Ferraro *et al.* (38) showed that muscle contraction were significantly reduced using multiple electrode arrays which consisted of 16 needles.

Although detailed modeling of electric field distribution in tissue have been introduced and are used in electroporation treatments planning (24, 25, 42-47), limited attention is paid to the modeling of the low strength electric field distribution in the non-target tissues, in both reversible and irreversible electroporation applications.

The goal of this paper is to perform a mathematical analysis of muscle contraction inducing low strength electric field distribution around the electroporation treated area and to investigate the effect of electrode design on these fields. The study is focused on analyzing electric fields strengths that are relevant to denerved muscle activation threshold (48). We analyzed the effects of typical clinical electroporation electric pulse sequences and electroporation electrode design. The

analysis shows that the volume of tissue affected by muscle activation electric fields during typical clinical electroporation protocols and with typical electroporation electrodes design is very large. However, we find that certain electrode configurations exist that may significantly reduce the volumes of non-target tissues affected by electric fields strong enough to induce muscle contraction outside the electroporation treated volume, without affecting the electroporation process in the targeted volumes. We have identified one such configuration that we named "Current Cage". In this study we analyzed the Current Cage configuration advantage over conventional electrode designs for NTIRE and skin electroporation applications, through mathematical modeling and with an experimental study on a tissue phantom.

Materials and Methods

When muscle tissue is exposed to electric fields than sensation, muscle contraction, thermal effect, reversible and irreversible electroporation may take place depending on field strength and time of exposure to the field (49). The threshold for denerved muscle contraction is about of 5 V/cm (48), while the threshold for irreversible electroporation is more than two orders of magnitude higher (46). In this study we propose that for electroporation treatment planning it is important to know both, the volume of tissue that is subjected to electroporation inducing electric fields (V_{ep}) as well as the volume of tissue that will experience electric fields above the muscle contraction threshold (V_{MC}). Theoretical studies were performed with numerical analyses that used the finite element method (FEM) implemented in COMSOL Multiphysics (Version 3.5a, COMSOL, Sweden) and MATLAB (Version 7.1a, Mathworks, USA) software. FEM is commonly used for optimization of electroporation pulse parameters and electrode configuration design (24, 43, 47, 50). Some numerical results were validated with experimental studies on tissue phantoms.

Theoretical Study

Mathematical Formulation: In current electrochemotherapy and NTIRE electroporation procedures the pulse lengths are longer than the cell membrane charging time, which is about 1 μsec (51); thus, a steady state DC analysis can be used to study electric field spatial distribution during the pulse application. In this part of the study we used the Laplace steady state equation,

$$\nabla\left(\sigma\left(\varphi\right)\right)=0 \qquad [1]$$

where, σ [S/m] is the local conductivity and φ [V] is the local potential.

To determine the electrical potential in the analyzed region Equation [1] is solved subject to boundary condition, which are:

$$\varphi\left(\Sigma_1\right)=V_0 \qquad [2]$$

$$\varphi\left(\Sigma_2\right)=0 \qquad [3]$$

where Σ_1 Σ_2 are the geometrical locations of the electroporation electrode boundaries.

Boundary conditions that do not relate to the electrodes are handled as electrical insulating boundaries:

$$n\cdot J=0 \qquad [4]$$

Where, J is an electrical current density vector (A/cm^2) and, n, is a vector normal to the surface.

The solution to Equations [1] to [4] yields the electric field distribution in the treated tissue. The post processing integration calculates the volumes of tissue, which are exposed to the electric fields of interest.

The goal of the treatment planning optimization process, developed in this study, will be to maximize the V_{ep} and at the same time reduce the $V_{MC}\cdot V_{MC}$ was defined in this model as the volume of tissue in which $E > 5$ V/cm. It should be emphasized that maximizing the V_{ep} value is not necessarily the optimal design, because the shape of the electroporated volume relative to the targeted tissue is of key interest. Moreover, experimental data and reported on models show that dynamic changes in conductivity take place in tissue due to the application of strong electric fields (52-54). In addition, tissues have a complex structure leading to heterogeneous conductivity in the treated area that affects the distribution of the electric fields (55). Nevertheless, the goal of this work is to analyze the relationship between the volumes of electroporation and of non-target tissue, which is exposed to muscle contraction inducing electric fields as a first step towards V_{MC} cognizant treatment planning. Therefore, we assumed the homogeneous tissue with a constant conductivity.

Numerical Model: First, we performed a basic analysis on two electroporation systems. First, we analyzed a standard system that is composed of two electrodes, currently used for NTIRE application (56). Second, we investigated a configuration we converged on from the analysis of various possible designs. We refer to this configuration as "Current Cage".

Then, we compared the proposed "Current Cage" electrode design with the commercially available skin electroporation 8 electrode array.

Two Electrode System

Geometry and Meshing: In this part of the study, the analyzed tissue was modeled as a homogeneous cylinder. The electrodes were modeled as cylinders of various lengths, h, completely inserted in the tissue. Figure 1 describes the system geometry and meshing.

Boundary Conditions and Solution

In this model we used a static analysis. A potential of 3000 V was applied on one electrode, while the second electrode was grounded. Tissue conductivity was assumed to be 0.2 S/m. V_{ep} was defined in this model as the volume of tissue in which $E > 800$ V/cm. The depth of penetration of both electrodes (the value of h) was changed from 1 to 5 cm with 1 cm increments and the V_{ep} and V_{MC} were calculated.

Current Cage Analysis: In this part of the study we investigated an electrode configuration, we refer to as Current Cage. In this specific configuration the positive electrode is located in the center of a circular array of external electrodes. An important aspect of this study is that the penetration of the central electrode in the treated tissue was varied relative to the penetration of the electrodes in the surrounding array.

Geometry and Meshing

The tissue was modeled as a homogeneous cylinder. The Current Cage consists of two elements. The first element is the surrounding electrodes, whose depth of penetration (h) was taken constant. The second element is the central, electrode which has a variable depth of penetration, D, relative to the surrounding electrodes. Figure 2 describes the system geometry and shows the mesh used in the analysis.

Boundary Conditions and Solution

For this model we used a static electric field COMSOL solver. A potential of 3000 V was applied on the central electrode, while the surrounding electrodes were grounded. In this study we tested the effect of the Current Cage radius (r), number of grounded electrodes (N) and the central electrode penetration depth (D) on V_{ep} and V_{MC}. Specifically, we tested cage exterior electrode radiuses (r) of 1, 1.5 and 2 cm. The number of surrounding electrodes (N) in the cage was 2, 4, 8, 16, 32 and 64. The penetration depth of the cage (h) was taken to be 4 cm (as a case study) and was kept constant. The penetration depth of the central electrode (D) was varied from 1 to 5 cm with 1 cm increments. The tissue conductivity was assumed to be 0.2 S/m.

Current Cage Analysis for Skin Electroporation Application: An important application of pulsed electric fields in medicine is for skin electroporation (57, 58), where significant efforts are made towards the reduction of muscle contractions (18, 38). In one commercial design for skin electroporation design pulses are applied through needle electrodes arranged in a two parallel row electrode array configuration (4-10 electrodes in a row) (15, 18). Another commercial design used for skin electroporation resembles in structure the Current Cage design studied here. However, it uses the same length electrodes in the center and in the surrounding electrodes (D = h) (44).

Geometry and Meshing

We compared a standard skin electroporation system (AgilePulse™ system, Harvard Apparatus, Hollison, MA) of an 8 electrodes array (Figure 3A) with 24 electrodes Current Cage configuration proposed in this study (Figure 3B).

Boundary Conditions and Solution

For this model we used a static electric field COMSOL solver. In the simulation of the parallel row electroporation system

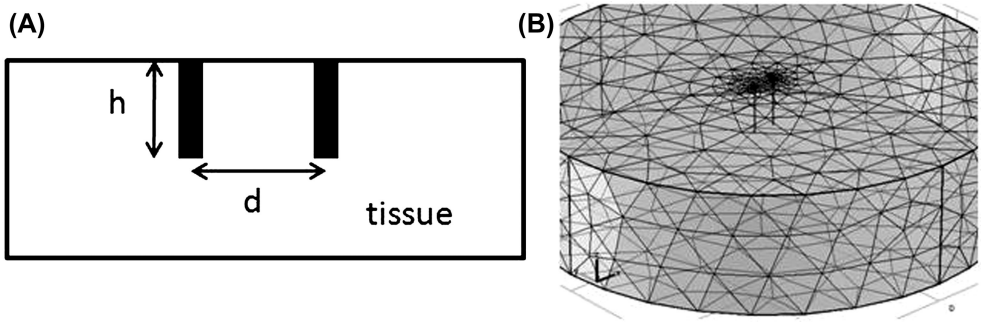

Figure 1: (**A**) Two electrodes system basic geometry. The analyzed tissue is modeled as a cylinder with 30 cm radius and 10 cm height. The electrodes are modeled as cylinders with 0.4 mm radius of variable length (h), d is a distance between the electrodes. (**B**) Two electrode system mesh. Mesh consists of 41986 tetrahedral elements. Mesh element size: 0.32-4 cm.

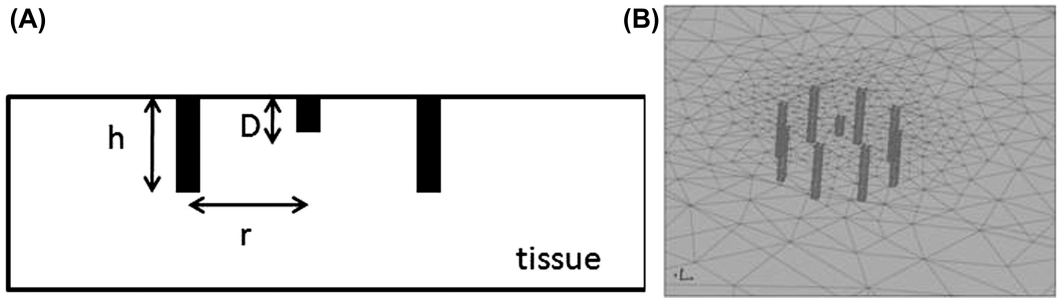

Figure 2: (**A**) Current Cage system basic geometry. The analyzed tissue is modeled as a cylinder with 30 cm radius and 10 cm height. The Current Cage Surrounding electrodes are modeled as cylinders with 0.4 mm radius and 4 cm length (h). The cage radius (r) is a radius of the treatment. The Current Cage Central electrode cylinder with 0.4 mm radius, variable length (D). (**B**) Current Cage system mesh. Mesh consisted of 77818 tetrahedral elements. Mesh element size: 0.32-4 cm.

we applied 450 V on 4 collinear electrodes and ground on the other four collinear electrodes. In the simulation of the Current Cage configuration we applied 900 V on the central electrode in the Current Cage 24 electrodes array. The geometry of the 24 electrodes Current Cage and the applied voltages were chosen in such a way that the electroporated volume (V_{ep}, volume where E>600 V/cm (57)) was equal to the V_{ep} in the commercial 8 electrodes parallel array. The dermis tissue conductivity was assumed to be 0.2 S/m.

Experimental Studies on Tissue Phantom

Tissue Phantom: A tissue phantom was prepared from agar gel. 0.2 g/L NaCl (Spectrum Chemical, Mfg Corp, CA), 30 g/L Agar (Becton, Dickison and Company, NJ were dissolved in 250 ml of distilled water and heated at 121°C in an autoclave for 15 minutes. The cooled mixture was poured into a 150 mm petri dish to form a gel slab with a conductivity of 0.2 S/m.

Electrode System Design: Two electrode systems were compared in this study. The first system consisted of two electrode needles (21G needles with cut edges) inserted in parallel, vertical to the gel slab surface at a 8mm distance between the needle centers. The second system is a Current Cage prototype. In this study we used a 16 electrodes Current Cage system. A 1.6 cm diameter Current Cage electrode array was manufactured using a Perspex "square" (2 cm by 2 cm) basis. 16 holes (0.4 mm) were drilled around an 8 mm radius circle for the external electrodes placement. One hole was drilled in the center of the circle for the central electrode placement. Electrodes were made from 21G needles with cut edges. All the external electrodes were connected to a single electrical output. To vary the penetration depth 1 mm step marks were engraved on the central electrode. The central electrode was connected to the positive outlet of a pulse generator and the external electrodes were connected to the ground outlet of the pulse generator. The schematic representation of the experimental system is shown in Figure 4.

Pulse Electric Field Application and Electrical Measurements: Electrical pulses of 400 V amplitude, 100 µs duration were delivered by a BTX model ECM 830 square-wave electroporator (Harvard Apparatus, MA) through the

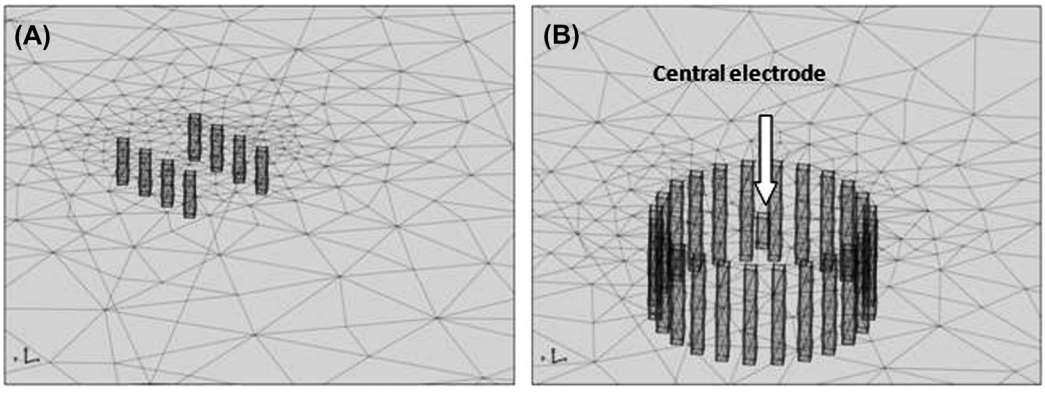

Figure 3: Skin electroporation. The analyzed tissue is modeled as a cylinder with 20 cm radius and 10 cm height (**A**) BTX 8 electrodes parallel array. Cylinders with 0.3 mm radius and 2 mm height. Electrodes are separated by 1.5 mm in row. The parallel rows are separated by 4 mm. Mesh consisted of tetrahedral 35523 elements. (**B**) Current Cage 24 electrodes array. Current Cage r = 4 mm. External electrodes were modeled as cylinders with 0.3 mm radius and d = 2.5 mm. Central electrode was modeled as cylinder with 0.3 mm radius and D = 1.3 mm. Mesh consisted of 34190 tetrahedral elements. Element size: 0.32-4 cm.

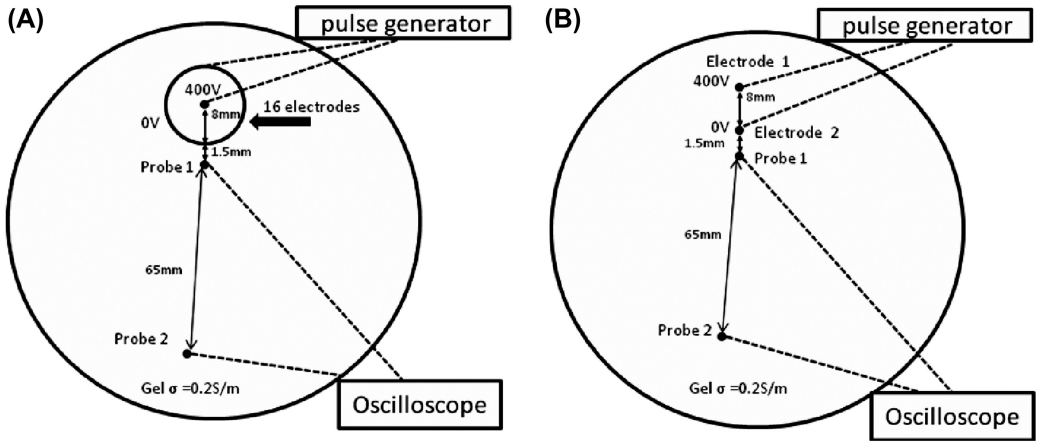

Figure 4: Experimental system scheme (**A**) Current Cage 16 electrode system. External electrode penetration was 8 mm and was constant during the experiment. Central electrode Penetration Depth varied from 1 to 10 mm. (**B**) Two electrodes electroporation system. Penetration Depth of both electrodes varied from 1 to 8 mm. The penetration depth of Probe 1 was 2 mm in all measurements.

electrode systems described in the previous paragraph. Single pulse was delivered for each experimental set up. The electric potential outside the area targeted for electroporation, was measured by a high impedance Tektronix TDS 210 oscilloscope (Tektronix, Inc, OR, US) between a small probe (30G needle with a cut edge) located 1.5 mm behind the negative electrode, at 2 mm penetration depth, and another similar probe located 65 mm behind the negative probe (see schematic in Figure 4), at 2 mm penetration depth (Figure 4). The potential difference outside the area targeted for electroporation was measured as a function of penetration depth of the two electrode system and as a function of the penetration depth of the central probe in the 1.6 cm Current Cage system. The penetration depth of the external electrodes in the current cage system was 8 mm and was kept constant during the experiment.

Results

The Two-Electrode System

Figure 5 shows the results of the analysis of electroporation induced electric fields in a two electrode system. Figure 5 shows the effect of the electrode penetration depth (h) and the distance between the two electrodes (d) on V_{ep} and V_{MC}. The simulation results indicate that increasing the distance between electrodes increases the volumes of tissue that experience muscle contractions (Figure 5A). Interestingly, the maximum of V_{ep} for the particular boundary conditions used in this analysis occurs when the electrodes are placed at d of 1.5 cm from each other, *i.e.* there is a local maximum (Figure 5B).

The Current Cage System

Figure 6 shows the effect of the Current Cage radius (r), number of external electrodes (N) and penetration depth (D) of the central electrode on V_{ep} and V_{MC}. The depth of penetration of the surrounding electrodes was 4cm and kept constant. Figure 6A, C and E show a strong correlation between the number of electrodes used in the external part of the Current Cage and V_{MC}. At the tested Current Cage radiuses (r = 1 cm, 1.5 cm and 2 cm) N equal or greater than16 significantly reduces the V_{MC} (Figure 6B, D, F), while V_{ep} was almost not affected by N and is dependent only on D (Figure 6B, D, F). In addition, we show that the penetration depth (D) of the central electrode to up to 3 cm does not affect V_{MC}, while V_{ep} increases with the increase in D. Furthermore, we show that a Current Cage radius of, r = 1.5 cm leads to larger V_{ep} than radiuses of r = 1 or 2 cm (Figure 6B, D, F).

Current Cage Analysis for the Skin Electroporation Application

We have performed a comparison between the commercial parallel electrode array and the Current Cage array for conditions in which the electroporation treated skin volume is the same. The reported electric field threshold for skin electropermeabilization (V_{ep}) is 600-1200V/cm (24, 59). The V_{MC} produced as a consequence of the production of the same V_{ep} for the two different configurations is given in Figure 7 and Table I.

Where:

V_{MC} [mm^3]- is the volume of tissue which is exposed to E>5 V/cm.

$V_{ep>600V/cm}$ [mm^3]- is the volume of tissue, which is exposed to E>600 V/cm (Minimum threshold for tissue permeabilization).

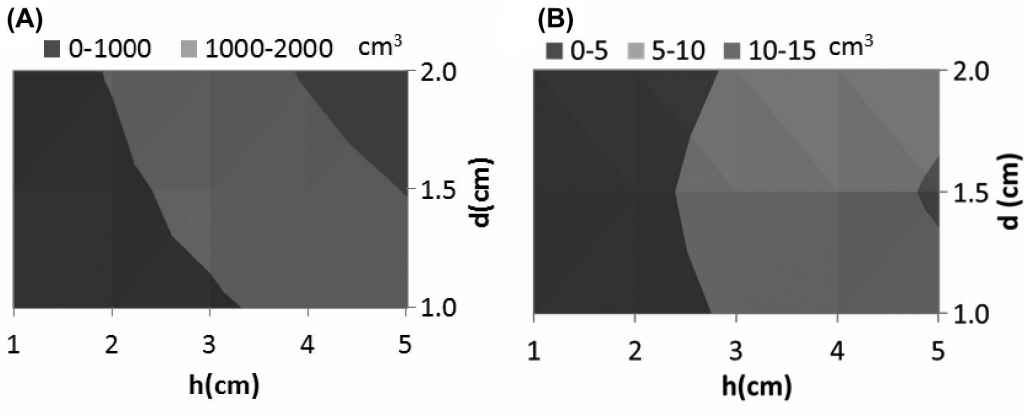

Figure 5: Surface plots (**A**) V_{MC} two electrode system. The plot shows the effect of Electrode Penetration Depth (h) and Distance between electrodes (d) on V_{MC}. (**B**) V_{ep} two electrode system. The plot shows the effect of Electrode Penetration Depth (h) and Distance between electrodes (d) on the V_{ep}.

$V_{ep>1120V/cm}$ [mm^3]- is the volume of tissue, which is exposed to E>1120 V/cm. (Full tissue permeabilization threshold).

The goal of 24 electrodes Current Cage was to decrease V_{MC} while keeping the same V_{ep} as in the BTX Parallel 8 electrode array.

Experimental Studies on Tissue Phantom: We have used the tissue phantom to compare experimentally the difference in the electrical potential generated outside the electroporation treated area between the "Two Electrode" and the "Current Cage" systems. The voltage measured by the oscilloscope is given in Table II.

From Table II it is evident that increasing the penetration depth increases the potential outside the electroporation treated zone in both systems. However, the Current Cage configuration reduces the electric field outside the Cage by an order of magnitude relative to the two electrode configuration.

Discussion

The problem of muscle contraction and pain is common to electric field based treatments such as NTIRE, electrochemotherapy, DNA vaccinations, defibrillation and electrostunning weapons (18, 19, 21, 37, 60, 61). The muscle fiber biological membrane, serves as a sensor for external triggers through the sustained transmembrane potential (62). Disturbing the transmembrane potential can, under certain condition, lead to action potential and muscle contraction (63), transforming of electro-chemical energy into force (64). However, extracellular electric field stimulation result in both action potential stimulation and ion channel blockage (63, 65, 66). Previous studies show that the discomfort and pain experienced by patients during electro therapies is caused in part, by involuntary muscle contractions (37, 67). Various chemical, physical and combined physical-chemical strategies have been proposed to reduce muscle contractions and pain in electrotherapies.

Physical methods for muscle contraction relaxation include use of ultra-short high frequency (ns) pulsed electric fields to arrest action potential propagation (34, 35, 65). In addition, pre-pulses of injected current, just before the main pulse delivery, were also shown to cause the reduction of muscle contraction, probably by partially depolarization of the membrane (68). Recently, it was proposed that cell sensitization to electric stimulation may be used to reduce muscle contractions (69). Moreover, increasing the frequency of delivered pulses to 5 kHz decreased the unpleasant feeling in humans in comparison with 1 Hz frequency; however, the pain intensity remained the same (37).

Although local and spinal injection of lidocaine reduced muscle contractions in electro stunning devices experiments (34); lidocaine injection alone did not prevent muscle contractions during electrochemotherapy (39-41) and NTIRE (unpublished). However, combined effect of shortening the pulse duration and emla cream topical application, decrease the strength of muscle twitches and increase the patient tolerance to the electroporation based DNA vaccination procedure (18).

Treatment planning and design are important for optimal clinical use of both reversible and irreversible electroporation. In reversible electroporation, mathematical models are employed to evaluate electric fields and mass transfer processes and to optimize the placement of electrodes to induce the desired mass transport in the targeted tissue volume. (43-47). In non-thermal irreversible electroporation the mathematical models are used to calculate the electric fields and temperature distribution in the targeted tissue volume and to optimize the placement of electrodes in such a way that the desired irreversible electroporation occurs without causing thermal damage (22, 24, 25).

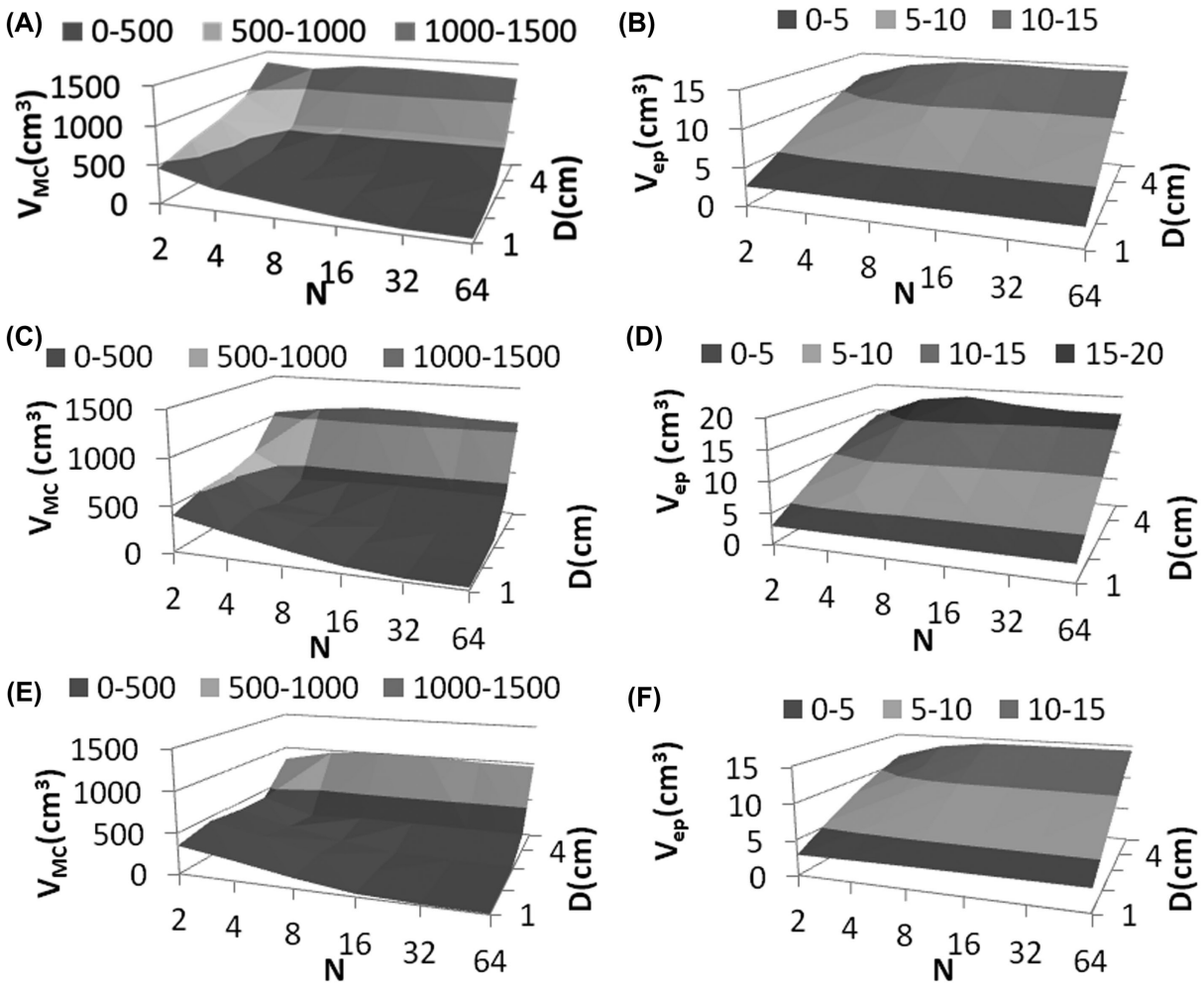

Figure 6: Surface plots V_{MC} and V_{ep} as a function of the number of electrodes (N) and penetration depth of the central electrode (D) in a Current Cage with r equal to (**A**) and (**B**) 2 cm, (**C**) and (**D**) 1.5 cm, (**E**) and (**F**) 1 cm.

Muscle contractions are inevitable during electroporation based treatment since the threshold for muscle activation is 2 orders of magnitude lower than the threshold for tissue electro permeabilization. This work shows that it may be useful to develop a better understanding of the entire range of electric fields that occur during electroporation, including those responsible for muscle contraction and pain. Computer simulations for spatial field distribution and excitation of nerves (70, 71), neuromuscular junction (72) and denerved muscles (73) were reported in the past. However, in this study we suggest that spatial field distribution in tissue should be analyzed and optimized as a part of electroporation treatment planning procedure.

Table I

Comparison of skin volumes that are exposed to threshold electric fields during electroporation.

	BTX parallel 8 electrode array	24 electrodes Current Cage
V_{MC} [mm^3]	15.09	2.90
$V_{ep>600V/cm}$ [mm^3]	0.11	0.11
$V_{ep>1120V/cm}$ [mm^3]	0.04	0.04
$V_{MC}/V_{ep>600V/cm}$	137	26
$V_{MC}/V_{ep>1120V/cm}$	410	73

In this work we propose a new electrode configuration – Current Cage, which we compared with the two-electrode system, currently used for electroporation procedures, and the commercially available Parallel 8 electrode array, used for skin electroporation.

The first study dealt with the classical electrode design for NTIRE in which two parallel needle electrodes are introduced into the targeted tissue. We investigated the effect of electrode configuration on V_{MC} and V_{ep}. Figure 5A shows that increasing penetration depth and distance between two parallel needle

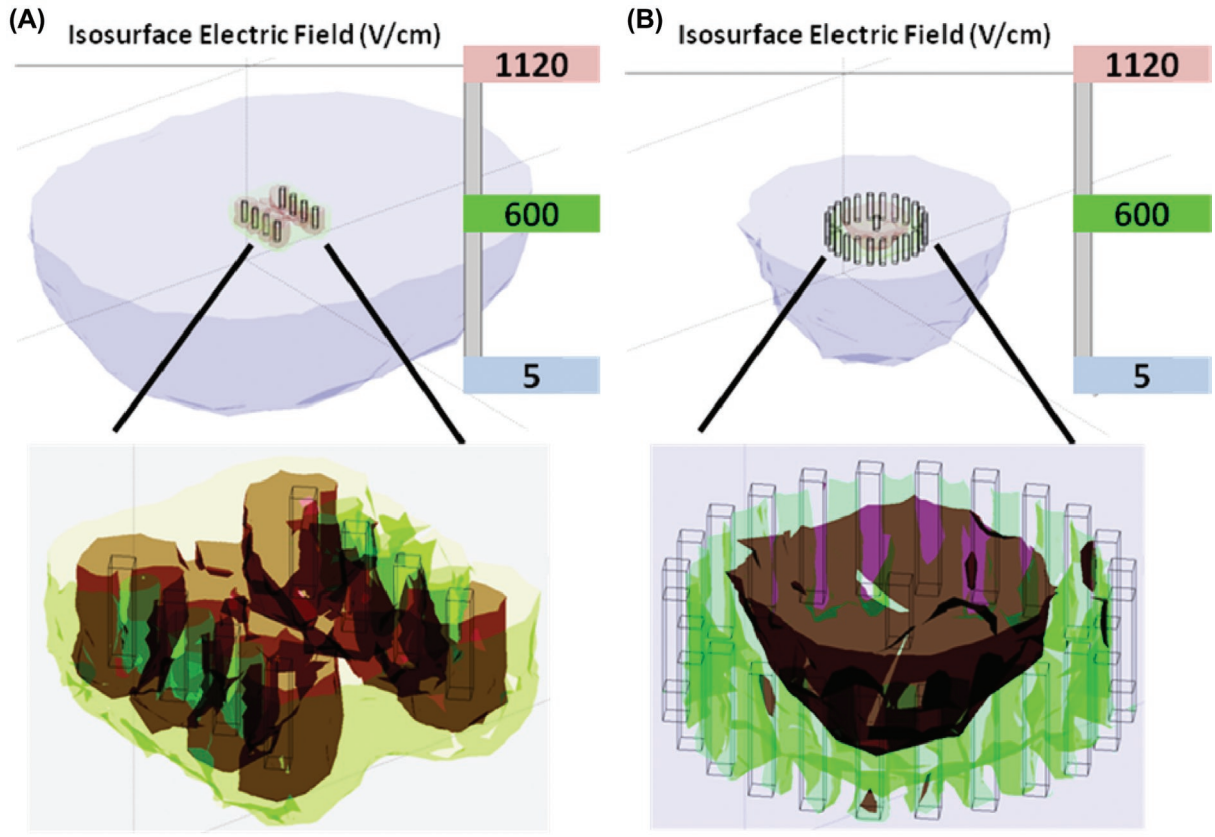

Figure 7: Skin electroporation. (**A**) V_{MC} and V_{ep} by a standard BTX Parallel 8 electrode array. (**B**) V_{MC} and V_{ep} by a 24 electrodes Current Cage system. V_{MC}- grey color, $V_{ep>600}$ green color, $V_{ep>1120}$ purple.

electrodes increases the V_{MC} and V_{ep}. Although the increase of the distance between two electrodes from 1 cm to 1.5 cm led to an increase of V_{ep}, further increase of the distance from 1.5 cm to 2 cm caused a reduction of V_{ep}. This result is consistent with (22). However, this result was shown here in a different type of data display from (22), which suggests that there may be an optimal electrode configuration for maximal tissue ablation volume and that the system response is not linear. It is also evident from the results that the volume of excited muscle tissue during typical electroporation procedures is substantial.

Next, we investigated the spatial distribution of electric fields in the proposed Current Cage design. The idea behind this design is based on the fact that in electroporation based treatment there is the need to produce electroporative electric fields strengths in a very specific volume (V_{ep}), while minimizing V_{MC}. The concept of a Current Cage design is based on previously reported sock-type electrodes used for defibrillation (74, 75). Although the sock-type electrode configuration was successfully implemented for the heart; the heart is a separate organ, relatively easy for de-entangling. In contrast, in electroporation based treatments the electrodes are usually inserted into the tissue. To our knowledge this is the first work that proposes the use of a Current Cage type electrode design for decreasing the exposure of tissues surrounding the electroporation treatment volumes to the low electric fields which cause tissue excitation.

Figure 6 shows the effect of the number of grounded electrodes in the external cage (N) and the penetration depth of the central electrode (D) on V_{MC} and V_{ep}, in Current Cages

Table II

Experimental comparison between Two Electrodes and Current Cage designs on tissue phantoms. h (mm) is the penetration depth of the electrodes in Two electrode system; D (mm) is the penetration depth in the Current Cage system, V (V) is the voltage read on the probe by oscill oscope.

Two electrodes design		Current Cage design	
H (mm)	V (volt)	D (mm)	V (volt)
1	148 ± 1.14	1	1.06 ± 0.09
2	165 ± 0.7	2	1.8 ± 0.1
3	174 ± 0.8	3	2.4 ± 0.12
4	181 ± 1.4	4	3.3 ± 0.17
6	199 ± 2.5	6	5.0 ± 0.28
8	201 ± 2.2	8	7.8 ± 0.5

of 1, 1.5 and 2 cm radius. Figure 6 shows that different from the two electrodes configuration (Figure 5), a current cage design may reduce V_{MC} while keeping the same V_{ep}. Figures 6A, C, E show that an increase of N (to 16 and more) and reduction of D decrease V_{MC}. In this study we used up to 64 electrodes for the Current Cage. However, further increase in the number of electrodes is possible and may be beneficial. For instance, Choi *et al.* (76) reported a manufacturing method for 256 electrodes for skin electroporation. Moreover, in specific situations, when the inclusion of the whole treated region is possible without penetration, for example eye electroporation, the electrode cylinder (N->∞) can be used as a Current Cage instead of the penetration electrodes. At the same time the V_{ep} does not depend on N and increases with larger values of D (Figure 6B, D, F). The Current Cage design of this study is different from previously proposed circle electroporation electrode arrays (38, 77), or circle electrode arrays with a positive electrode in the middle (44). The key difference is that in those designs all the electrodes have the same length. We find that when D is equal or larger than *h* the V_{MC} is significantly higher compared to the configuration when D is smaller than *h*. This observation can be explained by the Faraday cage nature of the Current Cage system. In an ideal Faraday cage, which fully encloses the treated region, there will be no external field outside the cage due to charge redistribution on the cage surface.

Next we compared the Current Cage system with the commercially available Parallel 8 electrode array. We assumed the threshold of skin permeabilization to be 600-1120 V/cm (24, 59) and compared the V_{MC} in the two systems for the same V_{ep} (Figure 7A, B and Table I). The analyses revealed that while the ratio of $V_{MC}/V_{ep>600\,V/cm}$ and $V_{MC}/V_{ep>1120\,V/cm}$ was 135 and 410 in the commercial Parallel 8 electrode array; it was 73 and 26 in the 26 electrodes Current Cage design (Table I). The $V_{ep>600\,V/cm,}$ and $V_{ep>1120\,V/cm}$ were the same in the both systems. It is important to point out that skin has a very complex structure that affects the distribution of the externally applied electric fields (24, 59). Although mechanical heterogeneity and dynamic electric properties are important parameters for electroporation planning (24, 55, 59), in this work we focused on the optimization of ratio the V_{MC} to V_{ep}. The methodology developed here, could be incorporated into the previously reported advanced electroporation models of skin, *e.g.* (24, 59).

Finally we experimentally compared the 16 Electrode Systems (8 mm treatment radius) with a Two Electrode system (8 mm distance between the electrodes). It is evident from Table II that the Current Cage design reduces the electric field outside the Cage by an order of magnitude. These experimental results suggest that the electric fields can be concentrated inside the pre planned treated area and demonstrate the advantage of the Current Cage design over the currently used two electrode method.

This study suggests including minimization of V_{MC} to the electrode configuration optimization pretreatment planning. We show that it is possible to design electrode configurations that can reshape the electric field distribution in the tissue in such a way as to reduce the volume of tissue affected by muscle contraction inducing electric fields without affecting the volume of tissue targeted with electroporation inducing electric fields. The minimization of V_{MC} can be easily incorporated into the existing electroporation treatment planning methodologies; for example (42, 43, 78, 79, 80).

The primary goal of this study was to introduce the concept of an electrode and illustrate its value. The study has made several simplifying assumptions and much work remains to be done. For instance, in this study we used a 5 V/cm threshold to calculate the V_{MC} and to introduce the cage concept. This, however, is the excitation threshold of a denerved muscle or muscle with blocked nerves. Nerve excitation threshold varies from 0.06 to 1 V/cm, where thinner fibers require higher field intensity for excitation (81). Therefore, the volume ratios for a criteria based on nerve excitation threshold will be different from those calculated in this study. Nevertheless, the fundamental principle of the cage design will produce conceptually similar results. It is important to also point out that in this work we simplified the tissue structure to a homogeneous medium; however muscle and nerves are anisotropic cells. It was shown that muscle cells electroporation depends on the orientation muscle cell with respect to the applied electric field (82). In addition, it was shown that nerve excitation also depends on the relation of the nerve fiber to the externally applied electric field (81). Future theoretical studies should incorporate the complex anisotropic nature of muscle and nerves. Furthermore, experimental validation of the cage concept is obviously required.

Conclusions

The effects of electroporation inducing electric fields on tissue are complex. These fields might cause undesirable nerve stimulation, muscle contraction and thermal damages in conjunction with the desired effects of electroporation. In this model we address the distribution of low amplitude electric fields which are sufficient to cause muscle contraction in the non-target tissues during electroporation treatments. The study shows that it is possible to reduce the volume of the non-target tissue affected by electric fields, which induce muscle contraction, through treatment planning and electrode design. We suggest that it would be beneficial to add reduction of non-target tissue volumes exposed to electric fields above muscle contraction in the treatment planning of DNA vaccination, electrochemotherapy and NTIRE and that

concepts such as the cage electrode design may be beneficial to this end.

Conflict of Interest Statement

The authors of this paper do not have any conflict of interest.

Acknowledgements

The authors acknowledge Angiodynamics Inc. for partial support of the study. The sponsor had not role in study design, the collection, analysis and interpretation of data; or in the writing of the manuscript; and in the decision to submit the manuscript for publication. The discretionary funds of BR were also used for partial support.

References

1. Neumann, E., Schaefer-Ridder, M., Wang, Y., Hofschneider, P. H. Gene transfer into mouse lyoma cells by electroporation in high electric fields. *EMBO Journal 1*, 841-845 (1982).
2. Pucihar, G., Krmelj, J., Rebersek, M., Napotnik, T., Miklavcic, D. Equivalent Pulse Parameters for Electroporation. *Biomedical Engineering, IEEE Transactions on 58*, 3279-3288 (2011).
3. Ongaro, A., Pellati, A., Caruso, A., Battista, M., De Terlizzi, R., De Mattei, M., Fini, M. Identification of In Vitro Electropermeabilization Equivalent Pulse Protocols. *Techology in Cancer Research and Treatment 10*, 465-473 (2011).
4. Schoenbach, K., Joshi, R., Beebe, S., Baum, C. A scaling law for membrane permeabilization with nanopulses. *Dielectrics and Electrical Insulation, IEEE Transactions on 16*, 1224-1235 (2009).
5. Mir, L. M. Therapeutic perspectives of in vivo cell electropermeabilization. *Bioelectrochemistry 53*, 1-10 (2001).
6. Titomirov, A. V., Sukharev, S., Kistanova, E. In vivo electroporation and stable transformation of skin cells of newborn mice by plasmid DNA. *Biochimica et Biophysica Acta 1088*, 131-134 (1991).
7. Okino, M., Mohri, H. Effects of a high-voltage electrical impulse and an anticancer drug on in vivo growing tumors. *Japanese Journal of Cancer Research 78*, 1319-1321 (1987).
8. Orlowski, S., Belehradek, J., Jr., Paoletti, C., Mir, L. M. Transient electropermeabilization of cells in culture. Increase of the cytotoxicity of anticancer drugs. *Biochemical Pharmacology 37*, 4727-4733 (1988).
9. Mir, L. M., Gehl, J., Sersa, G., Collins, C. G., Garbay, J.-R., Billard, V., Geertsen, P. F., Rudolf, Z., O'Sullivan, G. C., Marty, M. Standard operating procedures of the electrochemotherapy: Instructions for the use of bleomycin or cisplatin administered either systemically or locally and electric pulses delivered by the CliniporatorTM by means of invasive or non-invasive electrodes. *European Journal of Cancer 4*, 14-25 (2006).
10. Edhemovic, I., Gadzijev, E. M., Brecelj, E., Miklavcic, D., Kos, B., Zupanic, A., Mali, B., Jarm, T., Pavliha, D., Marcan, M., Gasljevic, G., Gorjup, V., Music, M., Vavpotic, T. P., Cemazar, M., Snoj, M., Sersa, G. Electrochemotherapy: a New Technological Approach in Treatment of Metastases in the Liver. *Technology in cancer research & treatment,* 475-485 (2011).
11. Mir, L. M., Orlowski, S. P. Mechanisms of electrochemotherapy. *Advanced Drug Delivery Reviews 35*, 107-118 (1999).
12. Jaroszeski, M. J., Dang, V., Pottinger, C., Hickey, J., Gilbert, R., Heller, R. Toxicity of anticancer agents mediated by electroporation in vitro. *Anti-Cancer Drugs 11*, 201-208 (2000).
13. van Drunen Littel-van den Hurk, S., Hannaman, D. Electroporation for DNA immunization: clinical application. *Expert Review of Vaccines 9*, 503-517 (2010).
14. Vasan, S., Hurley, A., Schlesinger, S. J., Hannaman, D., Gardiner, D. F., Dugin, D. P., Boente-Carrera, M., Vittorino, R., Caskey, M., Andersen, J., Huang, Y., Cox, J. H., Tarragona-Fiol, T., Gill, D. K., Cheeseman, H., Clark, L., Dally, L., Smith, C., Schmidt, C., Park, H. H., Kopycinski, J. T., Gilmour, J., Fast, P., Bernard, R., Ho, D. D. Electroporation Enhances the Immunogenicity of an HIV-1 DNA Vaccine Candidate in Healthy Volunteers. *PLoS ONE 6*, e19252 (2011).
15. Drabick, J. J., Glasspool-Malone, J., Somiari, S., King, A., Malone, R. W. Cutaneous Transfection and Immune Responses to Intradermal Nucleic Acid Vaccination Are Significantly Enhanced by in Vivo Electropermeabilization. *Molecular Therapy 3*, 249-255 (2001).
16. NIH. Clinical trials http://clinicaltrials.gov. Accessed Dec. 4, 2011. (2011).
17. Miklavcic, D., Pucihar, G., Pavlovec, M., Ribaric, S., Mali, M., Macek-Lebar, A., Petkovsek, M., Nastran, J., Kranjc, S., Cemazar, M., Sersa, G. The effect of high frequency electric pulses on muscle contractions and antitumor efficiency in vivo for a potential use in clinical electrochemotherapy. *Bioelectrochemistry 65*, 121-128 (2005).
18. Roos, A.-K., Eriksson, F., Walters, D. C., Pisa, P., King, A. D. Optimization of Skin Electroporation in Mice to Increase Tolerability of DNA Vaccine Delivery to Patients. *Molecular Therapy 17*, 1637-1642 (2009).
19. El-Kamary, S. S., Billington, M., Deitz, S., Colby, E., Rhinehart, H., Wu, Y., Blackwelder, W., Edelman, R., Lee, A., King, A. Safety and Tolerability of the Easy Vax[trade] Clinical Epidermal Electroporation System in Healthy Adults. *Molecular Therapy* (2011).
20. Rubinsky, B. *Irreversible Electroporation* (Springer, 2010).
21. Lee, E. W., Thai, S., Kee, S. T. Irreversible Electroporation: A Novel Image-Guided Cancer Therapy. *Gut Liver 4*(Suppl. 1), S99-S104 (2010).
22. Davalos, R. D., Mir, L. M., Rubinsky, B. Tissue ablation with Irreversible Electroporation. *Annals of Biomedical Engeneering 33*, 223-231 (2005).
23. Edd, J. F., Horowitz, L., Davalos, R. D., Mir, L. M., Rubinsky, B. In vivo results of a new focal tissue ablation technique: irreversible electroporation. *IEEE T Biomed Eng 153*, 1409-1415 (2006).
24. Pavselj, N., Miklavcic, D. Resistive heating and electropermeabilization of skin tissue during in vivo electroporation: A coupled nonlinear finite element model. *International Journal of Heat and Mass Transfer 54*, 2294-2302 (2011).
25. Garcia, P., Rossmeisl, J. J., Neal, R., 2nd, Ellis, T., Davalos, R. A Parametric Study Delineating Irreversible Electroporation from Thermal Damage Based on a Minimally Invasive Intracranial Procedure. *Biomedical Engineering Online* (2011).
26. Rubinsky, B. Irreversible electroporation in medicine. *Tech Cancer Res Treat 6*, 255-260 (2007).
27. Onik, G., Mikus, P., Rubinsky, B. Irreversible electroporation: implications for prostate ablation. *Technology in Cancer Research & Treatment 6*, 295-300 (2007).
28. Rubinsky, B., Onik, G., Mikus, P. Irreversible Electroporation: A New Ablation Modality - Clinical Implications. *Technology in Cancer Research and Treatment 6*, 37-48 (2007).
29. Garcia, P., Pancotto, T., Rossmeisl, J. J., Henao-Guerrero, N., Gustafson, N., Daniel, G., Robertson, J., Ellis, T., Davalos, R. Non-thermal irreversible electroporation (N-TIRE) and adjuvant fractionated radiotherapeutic multimodal therapy for intracranial malignant glioma in a canine patient. *Technol Cancer Res Treat 10*, 73-83 (2011).
30. Neal, R., 2nd, Singh, R., Hatcher, H., Kock, N., Torti, S., Davalos, R. Treatment of breast cancer through the application of irreversible

electroporation using a novel minimally invasive single needle electrode. *Breast Cancer Res Treat 123*, 295-301 (2010).
31. Thomson, K. in *Irreversible Electroporation* (Ed. B. Rubinsky) 249-254 (Springer, 2010).
32. Ball, C., Thomson, K., Kavnoudias, H. Irreversible Electroporation: A New Challenge in "Out of Operating Theater" Anesthesia. *Anesth Analg 110*, 1305-1309 (2010).
33. Deodhar, A., Dickfeld, T., Single, G. W., Hamilton, W. C., Thornton, R. H., Sofocleous, C. T., Maybody, M., Gonen, M., Rubinsky, B., Solomon, S. B. Irreversible Electroporation Near the Heart: Ventricular Arrhythmias Can Be Prevented With ECG Synchronization. *American Journal of Roentgenology 196*, W330-W335 (2011).
34. Despa, F., Basati, S., Zhang, Z. D., D'Andrea, J., Reilly, J. P., Bodnar, E. N., Lee, R. C. Electromuscular Incapacitation Results From Stimulation of Spinal Reflexes. *Bioelectromagnetics 30*, 411-421 (2009).
35. Joshi, R. P., Mishra, A., Xiao, S., Pakhomov, A. Model Study of Time-Dependent Muscle Response to Pulsed Electrical Stimulation. *Bioelectromagnetics 31*, 361-370 (2010).
36. Rogers, W. R., Merrit, J. H., Comeaux, J. A., Kuhnel, C. T., Moreland, D. F., Teltschik, D. G., Lucas, J. H., Murphy, M. R. Strength-Duration Curve for an Electrically Excitable Tissue Extended Down to Near 1 Nanosecond. *IEEE T Plasma Sci 32*, 1587-1599 (2004).
37. Zupanic, A., Ribaric, S., Miklavcic, D. Increasing the repetition frequency of electric pulse delivery reduces unpleasant sensations that occur in electrochemotherapy. *Neoplasma 54*, 246-250 (2007).
38. Ferraro, B., Heller, L. C., Cruz, Y. L., Guo, S., Donate, A., Heller, R. Evaluation of delivery conditions for cutaneous plasmid electrotransfer using a multielectrode array. *Gene Ther 18*, 496-500 (2011).
39. Sersa, G., Stabuc, B., Cemazar, M., Miklavcic, D., Rudolf, Z. Electrochemotherapy with Cisplatin: Clinical Experience in Malignant Melanoma Patients. *Clinical Cancer Research 6*, 863-867 (2000).
40. Rodriguez-Cuevas, S., Barroso-Bravo, S., Almanza-Estrada, J., Cristobal-Martinez, L., Gonzalez-Rodriguez, E. Electrochemotherapy in Primary and Metastatic Skin Tumors: Phase II Trial Using Intralesional Bleomycin. *Archives of Medical Research 32*, 273-276 (2000).
41. Heller, R., Jaroszeski, M. J., Glass, L. F., Messina, J. L., Rapaport, D. P., DeConti, R. C., Fenske, N. A., Gilbert, R. A., Mir, L. M., Reintgen, D. S. Phase I/II trial for the treatment of cutaneous and subcutaneous tumors using electrochemotherapy. *Cancer 77*, 964-971 (1996).
42. Zupanic, A., Miklavcic, D. in *Irreversible Electroporation* (Ed. B. Rubinsky) 203-222 (Springer, 2010).
43. Golberg, A., Rubinsky, B. A statistical model for multidimensional irreversible electroporation cell death in tissue. *BioMedical Engineering OnLine 9:13*, doi:10.1186/1475-1925X-1189-1113 (2010).
44. Sersa, G., Miklavcic, D., Cemazar, M., Rudolf, Z., Pucihar, G., Snoj, M. Electrochemotherapy in treatment of tumours. *EJSO 34*, 232-240 (2008).
45. Miklavcic, D., Corovic, S., Pucihar, G., Pavselj, N. Importance of tumour coverage by sufficiently high local electric field for effective electrochemotherapy. *EJC Supplements*, 45-51 (2006).
46. Miklavcic, D., Semrov, D., Mekid, H., Mir, L. M. A validated model of *in vivo* electric field distribution in tissues for electrochemotherapy and for DNA electrotransfer for gene therapy. *Biochim. Biophys. Acta 1523* 73-83 (2000).
47. Miklavcic, D., Snoj, M., Zupanic, A., Kos, B., Cemazar, M., Kropivnik, M., Bracko, M., Pecnik, E., Gadzijev, E., Sersa, G. Towards treatment planning and treatment of deep-seated solid tumors by electrochemotherapy. *Biomedical Engineering Online 9* (2010).
48. Sten-Knudsen, O. The ineffectiveness of the `window field' in the initiation of muscle contraction. *J Physiol 125*, 396-404 (1954).
49. Reilly, J. P. *Applied Bioelectricity: From Electrical Stimulation to Electropathology* (Springler, 1998).
50. Pavselj, N., Miklavcic, D. Numerical modeling in electroporation-based biomedical applications. *Radiology and Oncology 42*, 159-168 (2008).
51. Weaver, J. C. Electroporation of cells and tissues. *IEEE Transactions on Plasma Science 28*, 24-33 (2000).
52. Ivorra, A., Al-Sakere, B., Rubinsky, B., Mir, L. M. In vivo electrical conductivity measurements during and after tumor electroporation: conductivity changes reflect the treatment outcome. *Physics in Medicine and Biology 54*, 5949 (2009).
53. Pavselj, N., Bregar, Z., Cukjati, D., Batiuskaite, D., Mir, L. M., Miklavcic, D. The course of tissue permeabilization studied on a mathematical model of a subcutaneous tumor in small animals. *Biomedical Engineering, IEEE Transactions on 52*, 1373-1381 (2005).
54. Kos, B., Zupanic, A., Kotnik, T., Snoj, M., Sersa, G., Miklavcic, D. Robustness of Treatment Planning for Electrochemotherapy of Deep-Seated Tumors. *Journal of Membrane Biology 236*, 147-153 (2010).
55. Daniels, C., Rubinsky, B. Electrical Field and Temperature Model of Nonthermal Irreversible Electroporation in Heterogeneous Tissues. *Journal of Biomechanical Engineering 131*, 071006-071012 (2009).
56. *NanoKnife® System, http://www.angiodynamics.com/products/nanoknife*.
57. Gothelf, A., Gehl, J. Gene Electrotransfer to Skin; Review of Existing Literature and Clinical Perspectives. *Current Gene Therapy 10*, 287-299 (2010).
58. Denet, A.-R., Vanbever, R., Preat, V. Skin electroporation for transdermal and topical delivery. *Advanced Drug Delivery Reviews 56*, 659-674 (2004).
59. Pavselj, N., Miklavcic, D. Numerical Models of Skin Electropermeabilization Taking Into Account Conductivity Changes and the Presence of Local Transport Regions. *IEEE Transactions on Plasma Science 36*, 1650-1658 (2008).
60. Dosdall, D. J., Fast, V. G., Ideker, R. E. Mechanisms of Defibrillation. *Annu Rev Biomed Eng 12*, 233-258 (2010).
61. Joshi, R. P. Modeling Electrode-Based Stimulation of Muscle and Nerve by Ultrashort Electric Pulses. *IEEE T Plasma Sci 32*, 1687-1695 (2004).
62. Rassier, D. E. *Muscle Biophysics. From Molecules to Cells* (Springler, 2010).
63. Pumir, A., Romey, G., Krinsky, V. Deexcitation of Cardiac Cells. *Biophys J 74*, 2850-2861 (1998).
64. Rayment, I., Holden, H. M., Whittaker, M., Yohn, C. B., Lorenz, M., Holmes, K. C., Milligan, R. A. Structure of the actin-myosin complex and its implications for muscle contraction. *Science 261*, 58-65 (1993).
65. Joshi, R. P., Mishra, A., Song, J., Pakhomov, A. G., Schoenbach, K. H. Simulation studies of ultrashort, high-intensity electric pulse induced action potential block in whole-animal nerves. *IEEE Trans Biomed Engr 55*, 1391-1398 (2008).
66. Pakhomov, A., Kolb, J. F., Joshi, R. P., Schoenbach, K. H., Dayton, T., Comeaux, J., Ashmore, J., Beason, C. Neuromuscular disruption with ultrashort electrical pulses. *Proc SPIE-Int Soc Opt Eng 6219*, 621903-621910 (2006).
67. Delitto, A., Strube, M. J., Shulman, A. D., Minor, S. D. A Study of Discomfort with Electrical Stimulation. *Physical Therapy 72*, 410-421 (1992).
68. Horowicz, P., Schneider, M. F. Membrane charge moved at contraction thresholds in skeletal muscle fibres. *J Physiol 314*, 595-633 (1981).
69. Pakhomova, O. N., Gregory, B. W., Khorokhorina, V. A., Bowman, A. M., Xiao, S., Pakhomov, A. Electroporation-Induced Electrosensitization. *PLoS ONE 6*, e17100. doi:17110.11371/journal.pone.0017100 (2011).
70. Krastev, P., Tracey, B. in *Proceedings of the COMSOL Conference.*
71. Martinek, J., Stickler, Y., Reichel, M., Rattay, F. in *Proceedings of the COMSOL Conference.*
72. Long, G. L., Plescia, D., Shires, P. K. in *Proceedings of the COMSOL Conference* (Comsol).

73. Reichel, M., Mayr, W., Rattay, F. Computer simulation of field distribution and excitation of denervated muscle fibers caused by surface electrodes. *Artificial Organs 23*, 453-456 (1999).
74. Jayanti, V., Zviman, M. M., Nazarian, S., Halperin, H. R., Berger, R. D. Novel electrode design for potentially painless internal defibrillation also allows for successful external defibrillation. *J Cardiovasc Electrophysiol. 18*, 1095-1100 (2007).
75. Jayam, V., Zviman, M., Jayanti, V., Roguin, A., Halperin, H., Berger, R. D. Internal defibrillation with minimal skeletal muscle activation: a new paradigm toward painless defibrillation. *Heart Rhythm 2*, 1114-1115 (2005).
76. Choi, S.-O., Kim, Y., Park, J.-H., Hutcheson, J., Gill, H., Yoon, Y.-K., Prausnitz, M., Allen, M. An electrically active microneedle array for electroporation. *Biomedical Microdevices 12*, 263-273 (2011).
77. Spugnini, E. P., Citro, G., Porrello, A. Rational design of new electrodes for electrochemotherapy. *Journal of Experimental & Clinical Cancer Research 24*, 246-254 (2005).
78. Zupanic, A., Corovic, S., Miklavcic, D. Optimization of electrode position and electric pulse amplitude in electrochemotherapy. *Radiology and Oncology 42*, 93-101 (2008).
79. Zupanic, A., Corovic, S., Miklavcic, D., Pavlin, M. Numerical optimization of gene electrotransfer into muscle tissue. *Biomedical Engineering online 9:66*, doi:10.1186/1475-1925X-1189-1166 (2010).
80. Edd, J. F., Davalos, R. Mathematical Modeling of Irreversible Electroporation for Treatment Planning. *Technology in cancer research & treatment 6*, 275-286 (2007).
81. Reilly, J. Peripheral nerve stimulation by induced electric currents: Exposure to time-varying magnetic fields. *Medical and Biological Engineering and Computing 27*, 101-110 (1989).
82. Corovic, S., Zupanic, A., Kranjc, S., Al Sakere, B., Leroy-Willig, A., Mir, L., Miklavcic, D. The influence of skeletal muscle anisotropy on electroporation: in vivo study and numerical modeling. *Medical and Biological Engineering and Computing 48*, 637-648 (2010).

Received: October 20, 2011; Revised: December 7, 2011; Accepted: December 20, 2011